

A COMPARISON OF TROPOSPHERIC PATH DELAYS ESTIMATED IN PSI PROCESSING AGAINST DELAYS DERIVED FROM A GNSS NETWORK IN THE SWISS ALPS

Muhammad A. Siddique¹, Karina Wilgan², Tazio Strozzi³, Alain Geiger², Irena Hajnsek^{1,4}, Othmar Frey^{1,3}

¹Earth Observation and Remote Sensing, ETH Zurich, Switzerland

²Mathematical and Physical Geodesy, Institute of Geodesy and Photogrammetry, ETH Zurich, Switzerland

³Gamma Remote Sensing AG, Gümüli, Switzerland

⁴Microwaves and Radar Institute, German Aerospace Center - DLR, Oberpfaffenhofen, Germany

ABSTRACT

This paper reports the first results of a comparative study of tropospheric delays retrieved by means of PSI processing of an interferometric stack of SAR images against those derived independently from a permanent GNSS network. The stack comprises 33 Cosmo-SkyMed stripmap images acquired in the summers between 2008-13 over the Matter Valley in the Swiss Alps. The long-term objective of the study is to explore whether GNSS-derived delays from existing networks (i.e., not deployed specifically for a test site) in Swiss Alpine regions can aid in tropospheric phase corrections in SAR data, or rather the phase corrections derived within the PSI processing being at a higher spatial resolution might be appropriate to build upon the GNSS products by improving their resolution.

Index Terms— PSI, InSAR, tropospheric delays, GNSS

1. INTRODUCTION

The correction of troposphere-induced phase delays [1, 2] in repeat-pass interferometric SAR (InSAR) data stacks is typically necessary for the phase calibration of the stacks. Uncompensated delays would appear as erroneous deformation in case of differential interferometric analyses [3] or hamper focusing in case of tomography [4, 5]. The correction of these delays is particularly challenging in mountainous regions due to strong spatial variations of the local tropospheric conditions and topography-induced variations of the propagation paths. In these regions, both the turbulent mixing and vertical stratification of troposphere contribute to variable phase delays in the interferograms [5], contrary to regions of flat topography where only turbulent mixing effects are typically relevant [2]. In our earlier works [5, 6], a data-driven approach has been proposed to estimate and compensate the troposphere-induced phase delays. A persistent scatterer interferometric (PSI) analysis is performed; the delays are estimated within the PSI processing (with iterative refinement) while modeling the vertical stratification as a linear dependence on height. The contribution of turbulent mixing is considered in a stochastic sense. The spatial heterogeneity in

the delays is modeled as a random process, and its second-order statistics are inferred with a variogram estimation and parametric fitting process. In turn, regression-kriging is used to interpolate the delays estimated at PS locations over the scene to facilitate tomographic inversion along the elevation (perpendicular to line of sight) axis.

The performance of the aforementioned data-driven approach is influenced by the distribution of the PS in the observed scene. In a natural terrain such as the Swiss Alps, the PS distribution can be sparse which is not conducive. Therefore, it is useful to explore additional measures to aid the mitigation of tropospheric delays in mountainous regions. Global Navigation Satellite Systems (GNSS) stations are an auxiliary source of information on the influence of atmosphere [7]. In contrast to earlier works where the usefulness of assimilating GNSS-derived tropospheric delays in interferometric processing has already been shown for specific supersites, we explore a more general scenario in Swiss Alps (in the canton of Valais) where a few GNSS stations exist already and have not been deployed specifically for test purposes. We use these stations to estimate the tropospheric delays at the stations. These estimates are interpolated in time to correspond to SAR acquisition instants, and in space at PS locations. A comparison is performed between the GNSS estimates and the delays estimated within the PSI processing as a first step to objectively answer whether GNSS-derived delays can be used as a first correction of tropospheric delays (slow variations) in interferometry/tomography, or the PSI-based estimates (fast variations) can be used to improve the spatial resolution of the GNSS-derived delays.

2. METHODS

2.1. PSI processing

The PSI processing of the data stack is performed using the Interferometric Point Target Analysis (IPTA) [8] toolbox. A set of PS is iteratively identified using least squares regression with quality control at each iteration [9]. Among other phase contributions (e.g. residual topography and deformation), the

phase delays related to troposphere are isolated with appropriate spatio-temporal filtering and phase unwrapping.

In alpine regions, due to large variations in topography, a height-dependence of tropospheric phases needs to be considered. We adopt a multiple linear regression model as follows:

$$\psi(\mathbf{x}) = \mathbf{x}\boldsymbol{\beta} + \varepsilon(\mathbf{x}) \quad (1)$$

where ψ represents unwrapped (double-differenced) tropospheric phase for a given interferometric layer, and the vector $\mathbf{x} = [1 \ x_e \ x_n \ h]$. $\mathbf{x} \triangleq (x_e, x_n, h) = \mathbb{T}\{r, a, s\}$ represents 3-D location in map geometry in terms of easting, x_e , northing, x_n and height, h of the PS. $\mathbb{T}\{\cdot\}$ is the geocoding transformation applied on a range-azimuth-elevation tuple (r, a, s) . ε denotes the residue. $\boldsymbol{\beta}$ is the vector comprising regression coefficients which can be estimated with generalized least squares [10]:

$$\hat{\boldsymbol{\beta}} = (\mathbf{X}^T \mathbf{V}^{-1} \mathbf{X})^{-1} \mathbf{X}^T \mathbf{V}^{-1} \boldsymbol{\Psi} \quad (2)$$

where \mathbf{X} is the design matrix and $\boldsymbol{\Psi}$ is the vector of the tropospheric phases at PS locations:

$$\mathbf{X} = \begin{bmatrix} \mathbf{x}_1^T \\ \mathbf{x}_2^T \\ \vdots \\ \mathbf{x}_{N_{ps}}^T \end{bmatrix}, \quad \boldsymbol{\Psi} = \begin{bmatrix} \psi(\mathbf{x}_1) \\ \psi(\mathbf{x}_2) \\ \vdots \\ \psi(\mathbf{x}_{N_{ps}}) \end{bmatrix}. \quad (3)$$

\mathbf{V} is the data covariance matrix for the PS locations. The covariance model is estimated by computing a sample variogram for the residual phase in each interferometric layer [10, 5].

The tropospheric phases are converted to slant tropospheric delays (STD) as follows:

$$d\text{STD}_{\text{PSI}}(\mathbf{x}) = \frac{\lambda}{4\pi} \psi(\mathbf{x}). \quad (4)$$

These slant delays are double-differenced, i.e. they are relative to the reference point in the scene as well as relative to the master SAR image.

2.2. Least squares collocation using COMEDIE

Collocation of Meteorological Data for Interpretation and Estimation (COMEDIE) of tropospheric path delays is a software package developed at the Chair of Mathematical and Physical Geodesy, ETH Zurich, Switzerland [11]. This package contains tools to interpolate/extrapolate meteorological parameters such as temperature, air pressure and humidity, as well as zenith tropospheric delays (ZTD) and tropospheric refractivity, from real measurements to arbitrary locations. It allows least-squares collocation of parameters. It is useful for stochastic and deterministic interpolations, as well as screening of meteorological/tropospheric data. We use COMEDIE to interpolate (using spatial trends as well as data covariance

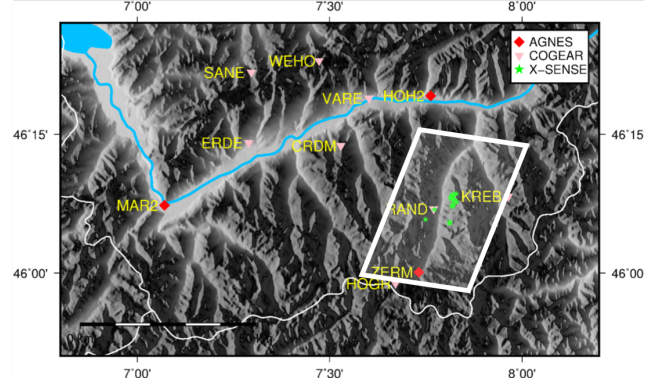


Fig. 1. The footprint of a SAR data set comprising CosmoSkyMed X-band acquisitions shown on top of the topography in map coordinates. The viewed scene covers parts of the Swiss Alps in the canton of Valais. The distribution of the GNSS stations in the area from different networks, viz. the AGNES network, the COGEAR network [13] and the X-Sense project [14] is also shown.

structure) the ZTD from GNSS stations in the observed scene to PS locations. Details of the tropospheric models used in COMEDIE are available in [12]. The predicated ZTD at PS location is then converted to STD as follows:

$$\text{STD} = \frac{1}{\cos \vartheta} \text{ZTD} \quad (5)$$

where ϑ is the incidence angle. These STD are converted to double-differenced delays:

$$d\text{STD}_{\text{GNSS}}(\mathbf{x}, t) = [\text{STD}(\mathbf{x}, t) - \text{STD}(\mathbf{x}, t_m)] - [\text{STD}(\mathbf{x}_r, t) - \text{STD}(\mathbf{x}_r, t_m)] \quad (6)$$

where t_m is the acquisition instant of the reference SAR image (single master), and \mathbf{x}_r is the location of the reference point in the scene. The $d\text{STD}_{\text{GNSS}}$ are then compared against $d\text{STD}_{\text{PSI}}$.

3. DATA

An interferometric stack comprising of 33 Cosmo-SkyMed stripmap images over Matter Valley in the Swiss Alps is used in this investigation. These X-band images are taken in the summers of 2008-13. Ionospheric effects on microwaves are frequency-dependent, and can often be ignored for high-frequencies such as the X-band [15]. Tropospheric delays are therefore the dominant component of the atmospheric delays for this stack. This region has several dormant as well as active landslides, rockslides, and rockfalls [16]. The topography varies between 1200–4000 m a.s.l..

Fig. 1 shows the footprint of the reference SAR acquisition over the topography in map coordinates. The distri-

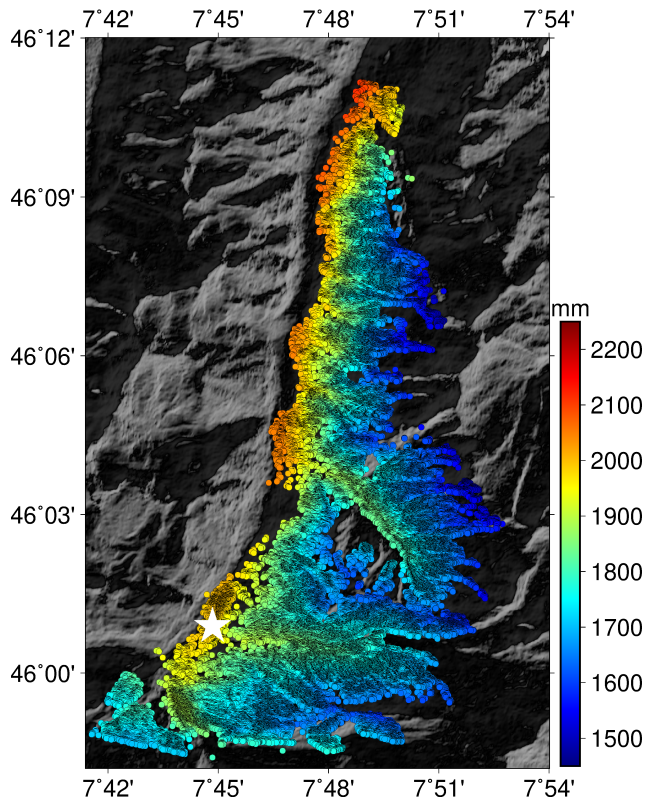


Fig. 2. GNSS-derived zenith tropospheric delays (ZTD) interpolated at PS locations, for the acquisition instant of the reference SAR image (2010-09-20, 17:46:45). The star in the figure marks the reference point.

Contributions of the GNSS stations in the area from different networks, viz. the Automated GNSS Network for Switzerland (AGNES), the Coupled Seismogenic Geohazards in Alpine Regions (COGEAR) network [13] and the X-Sense project [14], are also shown.

4. RESULTS

Fig. 2 shows ZTD interpolated at PS locations using COMEDIE, for the acquisition instant of the reference SAR image (2010-09-20, 17:46:45). These delays are subtracted from ZTD for each acquisition in the stack, and referenced to the selected reference point as well to obtain double-differenced delays. Fig. 3 shows a detailed comparison of the PSI-derived delays against those derived with GNSS for a selected interferometric layer. Fig. 4 shows a comparison of the regression coefficient along the height axis for all layers in the stack. For the case of GNSS, the estimates obtained with COMEDIE are fit with a linear dependence on height to obtain the regression coefficient. For the case of PSI, the coefficient is obtained using eq. 2.

5. DISCUSSION & OUTLOOK

The ZTD as shown in Fig. 2 for the reference data/time shows a dominant correlation with topography. This is expected since interpolations with COMEDIE include height dependence to model vertical stratification of the atmosphere. The spatial trends are typically smooth since the delays at PS locations are interpolated data values from the real measurements at the few GNSS stations in the observed scene. In Fig. 3, we see the comparison of estimated delays for a selected interferometric layer where there is a good agreement between the estimates from PSI and those from GNSS. The coefficient of determination $r^2 = 0.7$. However, for several layers, it is less than 0.3. The best case value is 0.8. Fig. 4 shows the estimated regression coefficient along height. We see that, for several interferometric layers, there is a good agreement among the values of the regression coefficient for the GNSS-derived and PSI-derived dSTD. This result hints towards the possibility of using GNSS-derived delays to support the mitigation of the stratification component of the tropospheric delays (e.g. to facilitate the phase unwrapping) in interferometric/tomographic processing. The results where X-Sense stations were available are also shown. A first analysis indicates that there is no clear improvement when using X-Sense stations in addition to the AGNES stations. It can be explained with the fact that these stations are closely spaced in height. Therefore, the sampling of the delay estimates with these stations is not widely spread in the height axis.

6. REFERENCES

- [1] R. Goldstein, "Atmospheric limitations to repeat-track radar interferometry," *Geophys. Res. Lett.*, vol. 22, no. 18, pp. 2517–2520, 1995.
- [2] R. F. Hanssen, *Radar interferometry: Data interpretation and error analysis*. Springer Science & Business Media, 2001, vol. 2.
- [3] G. Fornaro, "Tomographic SAR," *NATO SET-191 Lecture Series, Bucharest*, pp. 10–11, 2014.
- [4] S. Tebaldini and A. Guarnieri, "On the role of phase stability in SAR multibaseline applications," *IEEE Trans. Geosci. Remote Sens.*, vol. 48, no. 7, pp. 2953–2966, Jul. 2010.
- [5] M. Siddique, T. Strozzi, I. Hajnsek, and O. Frey, "A case study on the correction of atmospheric phases for SAR tomography in mountainous regions," *IEEE Trans. Geosci. Remote Sens.*, 2018.
- [6] M. Siddique, T. Strozzi, I. Hajnsek, and O. Frey, "A case study on the correction of atmosphere-induced phase disturbances for SAR tomography in mountainous areas," in *Proc. Europ. Conf. on SAR*, June 2018.
- [7] G. Fornaro, N. D'Agostino, R. Giuliani, C. Noviello, D. Reale, and S. Verde, "Assimilation of GPS-derived atmospheric propagation delay in DInSAR data processing," *IEEE J. Sel. Topics Appl. Earth Observ. Remote Sens.*, vol. 8, no. 2, pp. 784–799, Feb 2015.
- [8] C. Werner, U. Wegmüller, T. Strozzi, and A. Wiesmann, "Interferometric point target analysis for deformation mapping," in *Proc. IEEE Int. Geosci. Remote Sens. Symp.*, 2003, pp. 4362–4364.
- [9] U. Wegmüller, D. Walter, V. Spreckels, and C. Werner, "Nonuniform ground motion monitoring with TerraSAR-X persistent scatterer interferometry," *IEEE Trans. Geosci. Remote Sens.*, vol. 48, no. 2, pp. 895–904, Feb 2010.

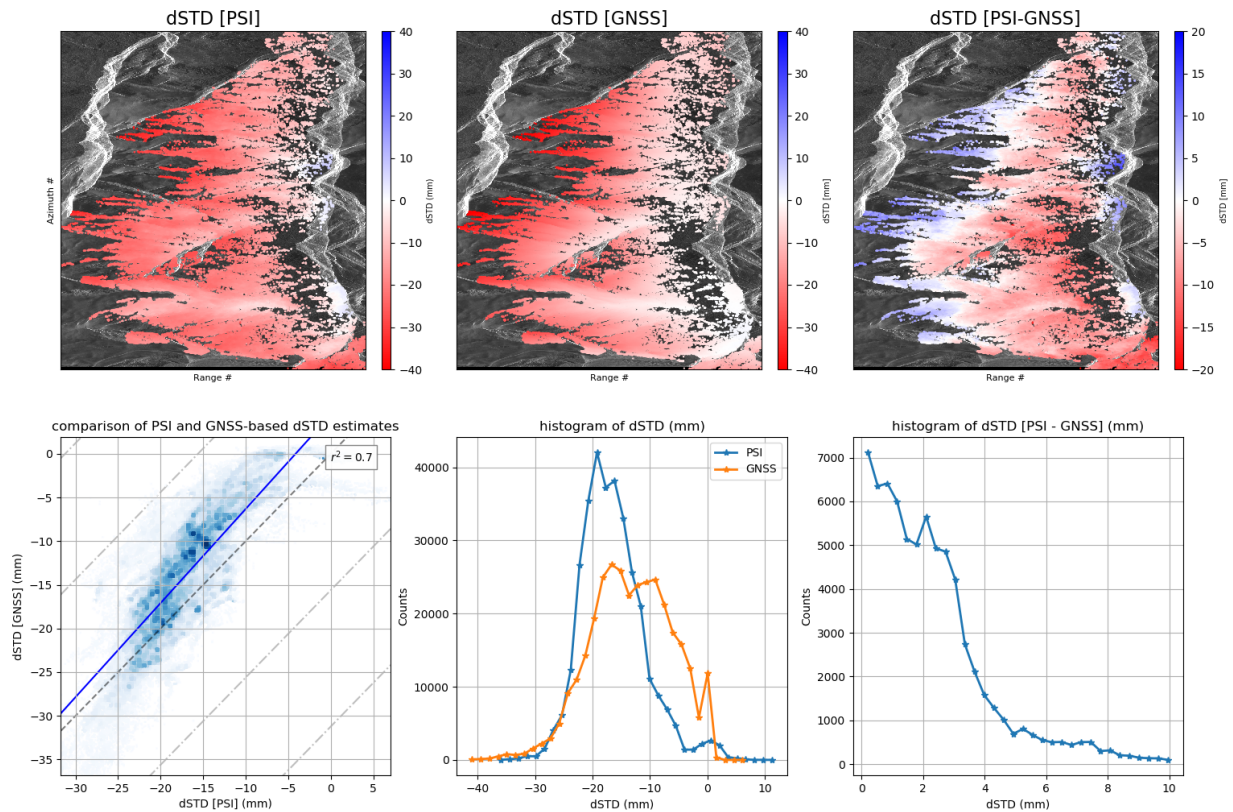


Fig. 3. Comparison of the PSI-derived tropospheric delays, $dSTD_{\text{PSI}}$ against those derived with GNSS stations, $dSTD_{\text{GNSS}}$ for an interferometric layer (slave: 2010-08-19, master: 2010-09-20). Top row shows the delays at PS locations in radar geometry. Bottom left: A scatter plot of the delays color coded according to their 2-D histogram. Bottom middle: 1-D delay histograms. Bottom right: Histogram of the difference ($dSTD_{\text{PSI}} - dSTD_{\text{GNSS}}$).

- [10] R. Bivand, E. Pebesma, and V. Gomez-Rubio, *Applied spatial data analysis with R*. Springer, 2008, vol. 747248717.
- [11] V. Eckert, M. Cocard, and A. Geiger, "COMEDIE: Collocation of meteorological data for interpretation and estimation of tropospheric pathdelays, Teil I: Konzepte, Teil II: Resultate, Teil III: Software," ETH Zurich, Tech. Rep. 194 and 195, 1992.
- [12] K. Wilgan, F. Hurter, A. Geiger, W. Rohm, and J. Bosy, "Tropospheric refractivity and zenith path delays from least-squares collocation of meteorological and GNSS data," *J. Geod.*, vol. 91, no. 2, pp. 117–134, 2017.
- [13] R. Delaloye, T. Strozzi, C. Lambiel, E. Perruchoud, and H. Raetzo, "Landslide-like development of rockglaciers detected with ERS-1/2 SAR interferometry," *Eur. Sp. Agency, (Special Publ. ESA SP)*, no. 649 SP, 2008.
- [14] J. Beutel, B. Buchli, F. Ferrari, M. Keller, M. Zimmerling, and L. Thiele, "X-Sense: Sensing in extreme environments," in *2011 Design, Automation & Test in Europe*. IEEE, 2011, pp. 1–6.
- [15] F. J. Meyer, "Performance requirements for ionospheric correction of low-frequency SAR data," *IEEE Trans. Geosci. Remote Sens.*, vol. 49, no. 10, pp. 3694–3702, 2011.
- [16] T. Strozzi, H. Raetzo, U. Wegmüller, J. Papke, R. Caduff, C. Werner, and A. Wiesmann, "Satellite and terrestrial radar interferometry for the measurement of slope deformation," in *Engineering Geology for Society and Territory-Volume 5*. Springer, 2015, pp. 161–165.

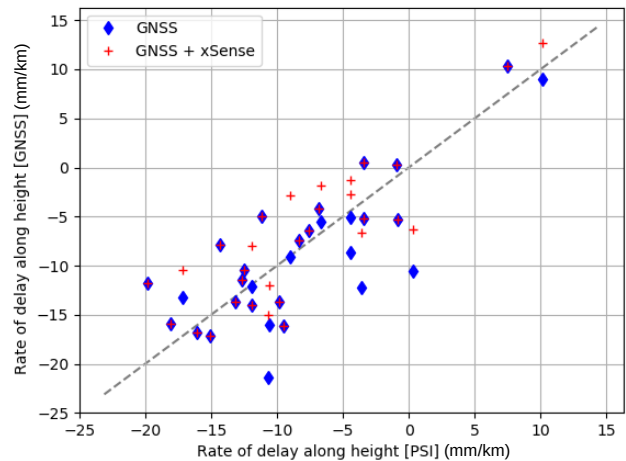


Fig. 4. Comparison of the regression coefficient along height for GNSS-derived tropospheric delays against those derived with PSI. Results when only the permanent AGNES GNSS stations are used are marked in blue. The red marks are the results when both the AGNES and X-Sense stations are used.